Spectral Substructure and Excitonic Interactions in the Minor Photosystem II Antenna Complex CP29 As Revealed by Nonlinear Polarization Spectroscopy in the Frequency Domain†

Bernd Voigt,*,‡ Klaus-Dieter Irrgang,§ Jürgen Ehlert,‡ Wichard Beenken,‡ Gernot Renger,§ Dieter Leupold,‡ and Heiko Lokstein||

Max-Born-Institut für Nichtlineare Optik und Kurzzeitspektroskopie, Max-Born-Strasse 2a, D-12489 Berlin, Germany, Max-Volmer-Institut für Biophysikalische Chemie und Biochemie, Technische Universität Berlin, Strasse des 17, Juni 135, D-10623 Berlin, Germany, and Institut für Biologie, Humboldt-Universität zu Berlin, Unter den Linden 6, D-10099 Berlin, Germany

Received July 17, 2001; Revised Manuscript Received January 8, 2002

ABSTRACT: CP29 (the *lhcb4* gene product), a minor photosystem II antenna complex, binds six chlorophyll (Chl) *a*, two Chl *b*, and two to three xanthophyll molecules. The Chl *a*/*b* Q_y absorption band substructure of CP29 (purified from spinach) was investigated by nonlinear polarization spectroscopy in the frequency domain (NLPF) at room temperature. A set of NLPF spectra was obtained at 11 probe wavelengths. Seven probe wavelengths were located in the Q_y spectral region (between 630 and 690 nm) and four in the Soret band (between 450 and 485 nm). Evaluation of the experimental data within the framework of global analysis leads to the following conclusions: (i) The dominant Chl *a* absorption (with a maximum at 674 nm) splits into (at least) three subbands (centered at 660, 670, and 681.5 nm). (ii) In the Chl *b* region two subbands can be identified with maxima located at 640 and 646 nm. (iii) The lowest energy Q_y transition (peaking at 681.5 nm) is assigned to a Chl *a* which only weakly interacts with other Chl *a* or *b* molecules by incoherent Förster-type excitation energy transfer. (iv) Pronounced excitonic interaction exists between certain Chl *a* and Chl *b* molecules, which most likely form a Chl *a*/*b* heterodimer. The subbands centered at 640 and 670 nm constitute a strongly coupled Chl *a*/*b* pair. The findings of the study indicate that the currently favored view of spectral heterogeneity in CP29 being due essentially to pigment−protein interactions has to be revised.

To achieve high efficiency of photosynthetic light transformation and optimal adaptation to different environmental, in particular, illumination, conditions, higher plants have evolved intricate antenna systems consisting of several light-harvesting pigment−protein complexes (LHCs).[1] The antenna system does not only increase the efficient cross section of the photosystems but also regulates excitation energy flow to the photochemical reaction centers. In plants the Chl *a*/*b* binding LHC subunits of the oxygen evolving photosystem II (PS II) are nuclear encoded by the gene family *lhcb 1-6*. The major and most peripheral component of the PS II antenna system is the trimeric LHC II (encoded by *lhcb 1-3* genes) that binds about 50% of the total Chl (*1*, *2*). LHC II is connected via minor complexes (encoded by the *lhcb 4-6* genes) to the Chl *a* binding core antenna subunits CP43 and CP47. The minor LHCs (also called CP29, CP26, and CP24) each bind about 5% of the total Chl (*1*, *2*).

Due to their location between LHC II and the core antenna the minor LHCs have been invoked to play key regulatory roles in the photosynthetic apparatus (*2*−*4*). The essential elementary process in the antenna system is radiationless electronic excitation energy transfer (EET) between the pigments. The nature of the EET steps depends on the electronic structure of the pigments, their spin state, and pigment−pigment as well as pigment−protein interactions (reviewed in refs *5* and *6*). The aggregation state of the subunits does not only effect the overall efficiency of EET but can (under light stress conditions) also introduce protective dissipative valves, as shown for LHC II aggregates (*7*).

Mechanistic understanding of the antenna function(s) requires detailed knowledge of the structural arrangement of the pigments within the protein matrix, in particular, the resultant strength of electronic coupling to other pigments. In the case of weak coupling, the energies of electronic transitions are influenced essentially by pigment−protein interactions, and EET occurs as an incoherent Förster-type hopping between the pigments. Interpretation of almost all EET studies on plant antenna complexes published so far relies on this concept (for recent reports see refs *8*−*12*). However, theoretical calculations taking into account information on the structure of LHC II with resolved positions

† Supported by the Deutsche Forschungsgemeinschaft (SFB 429, TPs A2 and A3).

* Author for correspondence. Tel: +49-30-6392 1352. Fax: +49-30-6392 1359. E-mail: voigt@mbi-berlin.de.

‡ Max-Born-Institut für Nichtlineare Optik und Kurzzeitspektroskopie.

§ Max-Volmer-Institut für Biophysikalische Chemie und Biochemie, Technische Universität Berlin.

|| Institut für Biologie, Humboldt-Universität zu Berlin.

[1] Abbreviations: Chl, chlorophyll; CP29 (CP26, CP24), *c*hlorophyll (binding) *p*rotein of MW 29 (26, 24) kDa; EET, excitation energy transfer; LHC, light-harvesting complex; NLPF, nonlinear polarization spectroscopy in the frequency domain; PS II, photosystem II.

10.1021/bi0155854 CCC: $22.00
Published on Web 02/06/2002

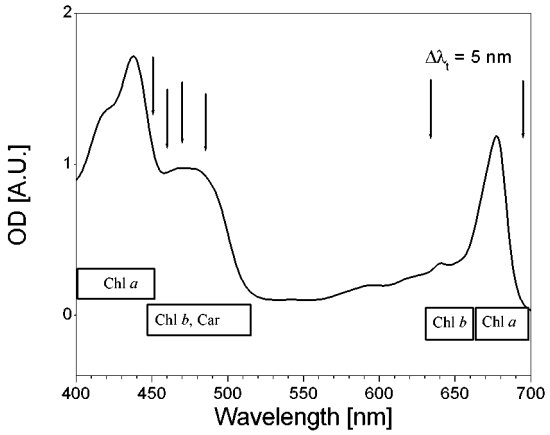

FIGURE 1: Absorption spectrum of CP29 at room temperature. Arrows indicate spectral positions of the probe wavelengths (λ_t) in the NLPF experiments; in the Q_y band λ_t were separated by 5 nm.

of the porphyrin rings (*13*) led to the conclusion that strong coupling may exist between individual pigments (*14*). Therefore, it seems premature to disregard effects that might arise from excitonic pigment−pigment interactions in LHCs. Major problems for unequivocal detection of excitonic coupling in pigment−protein complexes with multiple chromophores are the interference by effects such as inhomogeneous broadening (due to site-specific pigment−protein interaction) and spectral overlap of presumed subbands. Conventional techniques do not permit an unambiguous distinction. The method of nonlinear polarization spectroscopy in the frequency domain (NLPF) provides a suitable tool to address this problem (*15*−*17*).

Furthermore, to simplify interpretation of the data in the current study, we concentrate on the elucidation of spectral substructure and excitonic interactions in CP29. Obviously, CP29 is a much simpler system than LHC II and an appropriate model system for all LHCs because of the close similarity of essential structural motifs (*1*). CP29 binds about six Chls *a* and two Chls *b* (as compared to at least seven Chls *a* and five Chls *b* in LHC II). Additionally, xanthophyll molecules are bound to the complex, namely, lutein, neoxanthin, and violaxanthin; their exact stoichiometry, however, remains to be established. CP29 does not form (hetero) trimers as LHC II. The room temperature absorption spectrum of CP29 is shown in Figure 1. Certain regions of the spectrum can be assigned to different pigments. Chl *a* displays a broad Q_y absorption band between 660 and 680 nm peaking at 676.5 nm (*18*, *19*) and absorbs in the Soret region (B_x, B_y) at wavelengths shorter than 460 nm with a peak at 438 nm (*10*, *19*). In the Q_y region, Chl *b* exhibits a peak at about 640 nm and a weak shoulder near 650 nm. Additionally, vibronic states of Chl *a* are to be expected to form a broad but low-absorption underground in this region (*11*, *12*). In the Soret region, Chl *b* contributes (together with the xanthophylls) to an absorption band between 450 and 520 nm. However, also low-transition dipole moments bearing higher excited Chl *a* states have been predicted to be located in this region (*20*, *21*). A deconvolution of the CP29 room temperature Soret absorption spectrum reveals that the contributions of Chl *a* and *b* are well distinguishable (*10*); in particular, above 460 nm the contribution of Chl *a* can be neglected.

At low temperatures (4, 13 K) the absorption spectrum of CP29 exhibits more fine structure (*19*, *22*). The Chl *a* Q_y absorption narrows considerably, and the peak position is shifted from 676.5 to 674 nm. Below 13 K the Chl *b* absorption is characterized by two peaks at 638 and 650 nm. In the Soret region, the peak position of Chl *a* is nearly unchanged and that of Chl *b* is at 464 nm. Peaks attributed to xanthophylls were observed at 483 and 496 nm (*19*).

An unambiguous assignment of the above-mentioned spectral features to specific pigment binding sites in CP29 has not been achieved so far. Gaussian deconvolution of absorption spectra as well as linear and circular dichroism studies of CP29 resulted in up to nine Chl subbands (e.g., refs *18* and *23*). In these studies, the possibility of excitonic interactions between the pigments as a source of spectral heterogeneity has been considered but regarded as negligible on the basis of the interpretation of the data. Excitonic coupling may lead to energy level splitting, which may in turn result in the observed red shift of the absorption spectra for certain geometrical orientations of the interacting pigments (compare, e.g., ref *24*). In the case of strong electronic coupling the chromophores of the interacting unit share a common ground state for all excitonic transitions into the one-exciton state. Accordingly, EET does not occur via Förster-type "hopping" but as exciton downscattering. Several lines of experimental hints for excitonic coupling between Chl molecules in CP29 exist. For instance, circular dichroism spectra reveal a considerable rotational strength in the Q_y absorption band (*18*, *19*) that can hardly be explained without considering excitonic interactions. However, so far neither the exact number of excitonically coupled molecules has been determined nor have the involved subbands been identified (in particular not at physiologically relevant room temperature).

The present study analyzes the spectral substructure of the Q_y absorption band of CP29 using NLPF. As a result, unequivocal evidence for the existence of strong excitonic coupling in at least one Chl *a*−Chl *b* pair is obtained.

MATERIALS AND METHODS

CP29 was isolated from PS II membrane fragments prepared as outlined in ref *25* with the modifications as described in ref *26*. PS II membrane fragments were resuspended to 0.2 mg of Chl $a + b$ mL^{-1} in 0.8 M Tris-HCl (pH 8.35) under ambient light for 30 min. CP29 was extracted and purified following the protocol from ref *27* with the following modifications: 2 mM benzamidine and 1 mM Pefabloc (Merck) were used as protease inhibitors; sulfobetaine 14 was replaced by sulfobetaine 12. Chromatographic purification was performed on a CM-Sepharose Fast Flow column (Amersham Pharmacia Biotech) under dim green light at 4 °C. Elution buffers contained 0.1% (w/v) sulfobetaine 12 and 0.05% (w/v) *n*-dodecyl β-D-maltoside. One to two rechromatography steps were necessary to achieve the desired purity.

NLPF spectra were recorded by applying a 90° arrangement of pump (λ_p) and probe (λ_t) beams as introduced recently (*28*) and illustrated in Figure 2. Either λ_p or λ_t (both with a spectral width of about 0.05 cm^{-1}) is obtained from dye lasers (DCM/DMSO for the Q_y region and coumarin 102/methanol for the Soret region) simultaneously pumped by

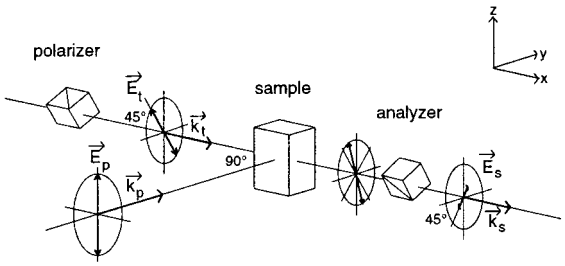

FIGURE 2: Principle of nonlinear polarization spectroscopy in the frequency domain (NLPF). Pump, probe, and signal fields (E) are distinguished by the indices p, t, and s, respectively, as well as the corresponding wavenumber vectors (k). The NLPF signal is the component of the signal field which is perpendicular to the incident probe field.

an excimer laser (pulse duration 15 ns). The sample (OD $\cong$ 1 at the maximum of the Q_y absorption) is located in a homemade flow system with a 5 mm quartz cell (Helma, Mülheim, Germany). At a laser repetition rate of 5 Hz the illuminated sample volume is exchanged after each flash. NLPF spectra were recorded in the low pump intensity range, thus satisfying the conditions for the description of NLPF spectra by a χ^3 approach. The photon flux density of the pump beam was about 4.5×10^{14} photon cm^{-2} pulse^{-1} for λ_t in the Q_y region and about 1 order of magnitude higher for λ_t in the Soret region. The intensity of the pump beam exceeded that of the probe beam by a factor of about 100. Absorption, circular dichroism, and fluorescence spectra of the samples were monitored before and after the NLPF experiments, indicating no sample degradation.

RESULTS AND DISCUSSION

Line Shape of the NLPF Signal for Model Systems. NLPF spectra are obtained at a fixed probe wavelength (λ_t) by tuning the pump wavelength (λ_p) across the absorption band under investigation. For an absorption band originating from only one homogeneously broadened optical transition (with the peak wavelength λ_0), the NLPF signal exhibits at least two features: (i) a spectrally narrow peak is observed in the immediate vicinity of λ_t, and (ii) a broad peak is centered at λ_0. A detailed description of the theoretical background of NLPF spectroscopy together with a thorough discussion of the contents of information in NLPF line shapes for the general case (overall absorption band consisting of inhomogeneously or homogeneously broadened subbands with varying degrees of electronic coupling) is given in ref *16*.

Nonidentical pigments (e.g., Chls *a* and Chls *b*) or identical pigments at energetically inequivalent binding sites give rise to a more or less substructured overall absorption profile of a pigment−protein complex.

In principle, the line shape of the resulting NLPF spectrum contains a series of distinguishable peaks (related to the spectral substructure). A global line-shape analysis comprising a fit of the theoretical NLPF line-shape function to a set of NLPF spectra obtained at different λ_t allows determination of the energy level scheme including energy relaxation and EET pathway(s) of the system under investigation. Fitting parameters are weighting factors, center frequencies, and dephasing rates for all subbands and matrices describing energy relaxation rates as well as the underlying term scheme. Algorithms for nonlinear optimization are used, e.g., according to Nelder and Mead. The procedure is described in detail in ref *16*.

Resulting from mutual distances, orientations, and strengths of transition dipole moments, three basic cases of pigment−pigment interactions within a protein matrix can be distinguished:

(i) Pigments are "isolated". (ii) Pigments are coupled by weak dipole−dipole interaction giving rise to only incoherent EET (Förster-type hopping). (iii) Strong dipole−dipole interaction between pigments leads to excitonic coupling which may result in splitting of the transition energies, redistribution of dipole strengths, and delocalization of the excitation energy. The strongly coupled pigments are also characterized by a common ground state.

Even if not discernible by conventional techniques the different modes of coupling can be distinguished by NLPF. To illustrate the potential of this technique, the expected NLPF line shapes for a simple system containing only two pigments characterized by two absorption bands with peak positions λ_1 and λ_2 will be outlined (Figure 3). The following characteristic features emerge in the NLPF spectra of such a system for the special cases that λ_t is located at the absorption maxima of the respective subbands, λ_1 and λ_2, whereas λ_p is tuned over the entire absorption profile.

(i) A system consisting of isolated pigments exhibits a *heterogeneous substructure* of the absorption profile. The corresponding NLPF spectrum shows in addition to the strong peak at the maximum of the subband in which λ_t is located another, less pronounced peak arising in the spectral region of the other subband (Figure 3C,D, solid lines). The contribution of the nonprobed subband to the overall NLPF signal depends on spectral overlap of the two subbands and scales with excited state lifetime. In case of no spectral overlap, the latter peak vanishes, and the NLPF spectrum features only the subband in which λ_t is located.

(ii) A system with weakly coupled pigments: The subbands represent independent species that are now connected via Förster-type EET (γ_{12}, Figure 3C,D, dotted lines). Probing in the higher energy subband results in almost the same NLPF line shape as in case i. Probing in the lower energy subband, the NLPF spectra are distinct: The peak in the spectral region of the higher energy subband grows with increasing EET rate. However, if there is no spectral overlap between the subbands (resulting also in vanishing EET), the NLPF spectrum features once more only the subband in which λ_t is located.

(iii) In case of strongly coupled pigments a *homogeneous substructure* emerges: The energy level scheme is characterized by a common ground state and two excitonic states with a transition rate (exciton downscattering), γ_{12}. In the NLPF profile, the peak of the nonprobed subband is considerably more pronounced than in the other two cases (Figure 3C,D, dashed lines). Since it can be assumed that the EET and relaxation rates from upper to lower states are higher than those in the reverse direction, the homogeneous substructure can be well distinguished from cases i and ii. Even if there is no spectral overlap between the two subbands, the peak of the NLPF spectrum corresponding to the nonprobed subband *does not disappear*. This effect originates from the bleaching of the *common* ground state of the two interacting species and, hence, allows *unequivocal* identification of heterogeneous and homogeneous substructure.

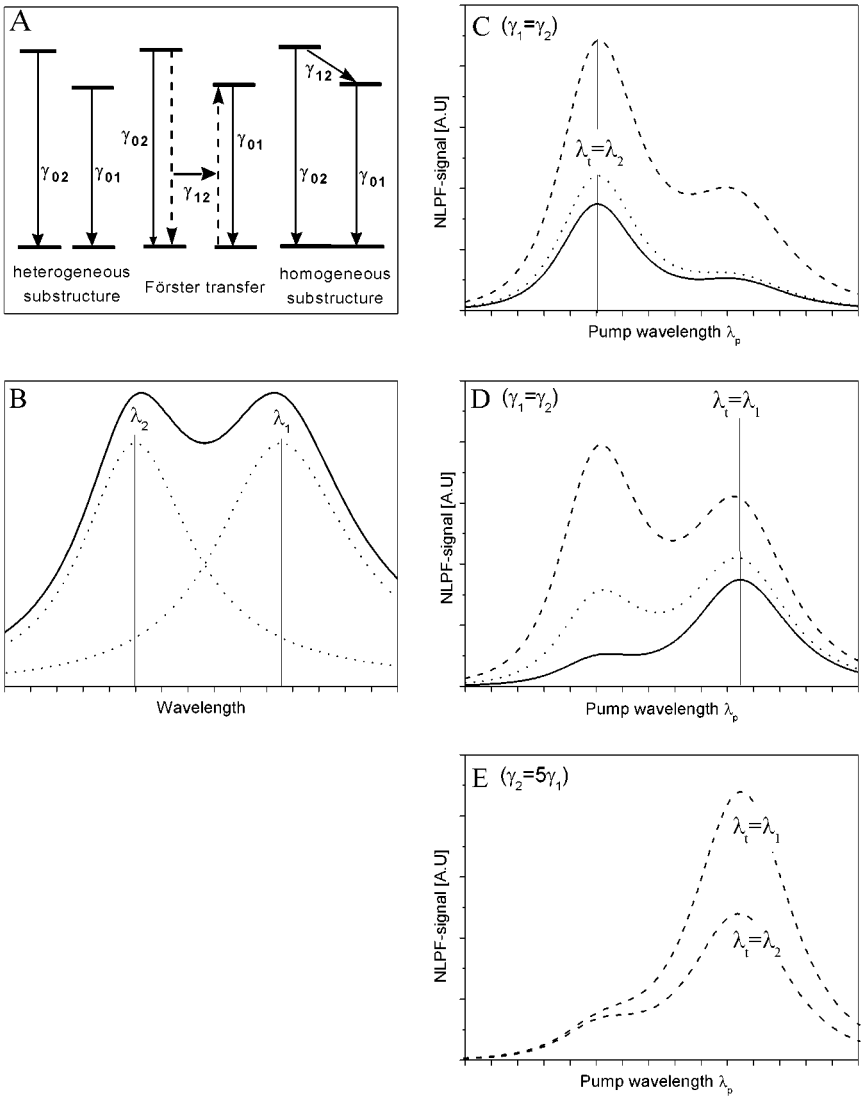

FIGURE 3: Theoretical line shapes of NLPF spectra of model systems (as depicted in panel A). The corresponding absorption spectrum is visualized in panel B. For the sake of simplicity, homogeneous line widths of both subbands as well as the spectral gap between them are assumed to be equal. The mutual orientation of the transition dipole moments is assumed to be parallel, and excited state lifetimes ($1/\gamma_{1,2}$, with $\gamma_{02} = \gamma_{12}$) are the same for both pigments (in panels B−D). Panels C−E: heterogeneous substructure, solid line; Förster-type excitation energy transfer, dotted line; homogeneous substructure (strong excitonic coupling), dashed line. Panel E visualizes the case that the higher energy subband has only one-fifth of the excited state lifetime of the other subband.

Note that the intensity of a NLPF subband scales with its excited state lifetime (*16*). Hence, if the latter is comparatively short, the corresponding subband may not be readily resolved in the overall NLPF spectrum regardless of the location of the probe wavelength. Figure 3E illustrates this issue for the homogeneous case; here the higher energy state has a shorter lifetime (one-fifth) than the lower energy state. The diminuition of the short-lived band is observed for the homogeneous (strong excitonic coupling) as well as the Förster-type EET case.

Antenna complexes such as CP29 contain more than two pigments (i.e., several Chls *a*, Chls *b*, and xanthophylls) that are incorporated into energetically inequivalent binding sites (resulting in inhomogeneous broadening) and may vary in coupling strength (through different mutual distances and orientations). Therefore, all cases (i−iii) can be expected to occur simultaneously in antenna complexes. Hence, the resulting line shape of the NLPF spectrum can be a complex superposition of the above outlined features. Nevertheless, NLPF spectra obtained by pumping in an energetically lower lying and probing in a higher energy absorption band, without spectral overlap (e.g., the Q_y and Soret bands, respectively), can provide invaluable information on excitonic coupling, in particular, between different pigment species, as will be shown below.

Nonlinear Polarization Spectroscopy in the Frequency Domain of CP29. NLPF spectra of CP29 (with λ_p tuned across the spectral range of the Chl *a* and *b* Q_y region, between 640 and 690 nm) were measured for different λ_t in the Q_y region. Normalized spectra as obtained for $\lambda_t = 640$, 650, 660, 670, 680, and 690 nm are displayed in Figure 4. Pronounced changes of spectral shape and shifting peak positions upon variation of λ_t are indicative of spectral heterogeneity of the Q_y absorption band. The displayed NLPF spectra obviously can be placed in two distinct groups: Variation of λ_t between 670 and 695 nm (right column in Figure 4) results in spectra peaking at 680 nm and displaying almost identical red wings. These observations most likely indicate the existence of a red-most subband (peaking at about 681 nm) connected by Förster-type EET, but not

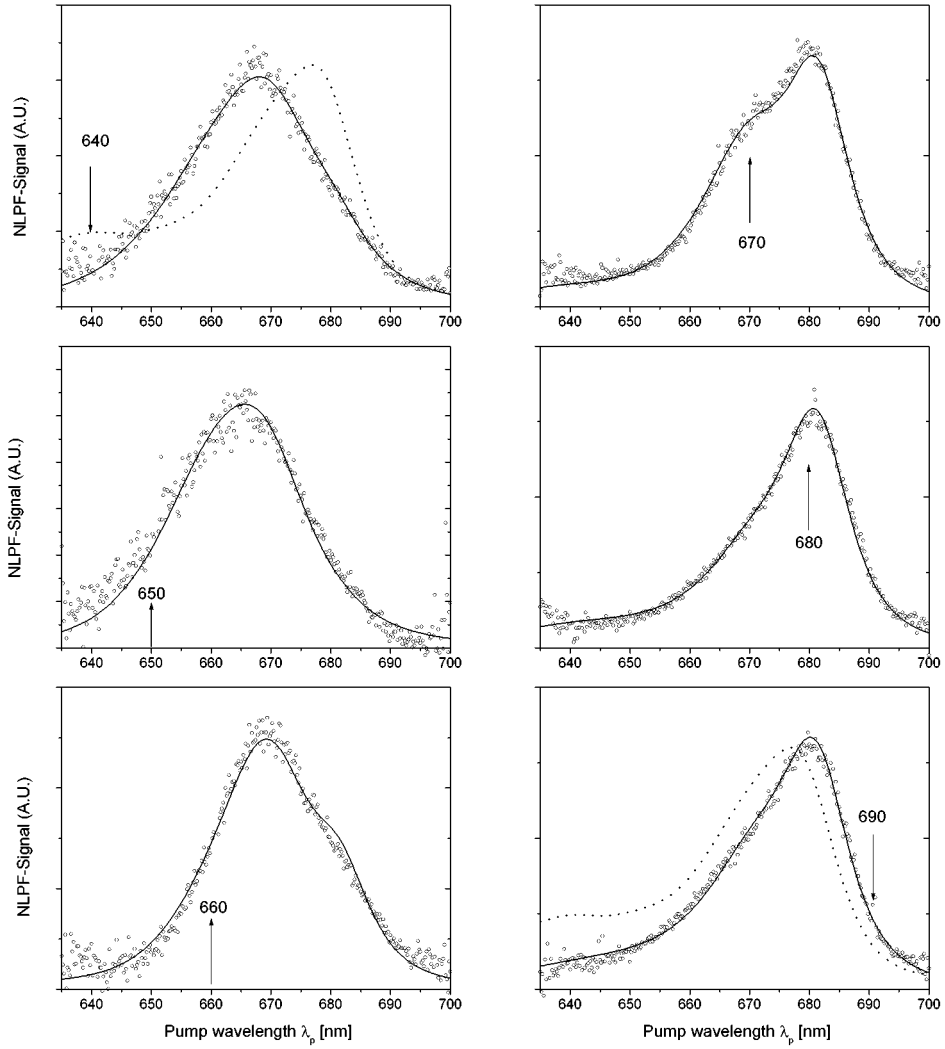

FIGURE 4: NLPF spectra of CP29 obtained at different probe wavelengths (λ_t, indicated by the arrows) in the Chl *a* and *b* Q_y region. All spectra were obtained at the same pump intensity. Solid lines: best fit of global data analysis. Dotted lines: absorption spectrum of CP29.

excitonically, to other subsystems at higher energy. Obviously, the shoulder on the blue wing of the spectrum obtained at $\lambda_t = 670$ nm reveals contributions of further (shorter wavelength) subbands. NPLF spectra obtained at λ_t between 640 and 660 nm display some variation in shape and position of the maximum (left column in Figure 4). In the framework of NLPF line-shape analysis this can be explained only as the result of superposition of several subbands (*16*), consistent with the proposed existence of further subbands in this spectral range (*18*, *23*). Subbands that can be assigned to Chls *b* are hardly observed in the NLPF spectra (in contrast to the absorption spectra) due to their short excited state lifetimes as compared to Chl *a* species.

NLPF spectra obtained by pumping *and* probing in the Q_y band provide hints for excitonic coupling. Whereas in the heterogeneous case the NLPF maximum shifts in parallel with shifting λ_t (*16*), here we observe that the maximum of the normalized NLPF signal for $\lambda_t = 650$ nm is blue shifted with repect to the one obtained for $\lambda_t = 640$ nm (Figure 5). This may well indicate excitonic interactions between species at about 640 and 670 nm.

It has to be noted that vibronic states of Chl *a* may overlap with Chl *b* Q_y states in this spectral region. However, the combination of their short lifetimes and low transition dipole moments marginalizes their contribution to the overall NLPF signal.

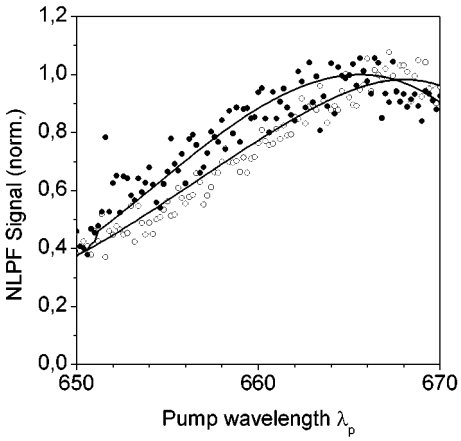

FIGURE 5: Direct comparison of normalized NLPF spectra of CP29 obtained at probe wavelengths (λ_t) 640 nm (open symbols) and 650 nm (closed symbols). Spectra were obtained at the same pump intensity.

To derive origin (excitonic versus nonexcitonic), actual number, and exact peak positions of the subbands from the set of NLPF spectra obtained at λ_t in the Q_y region is not straightforward. To ascertain the excitonic nature of sub-

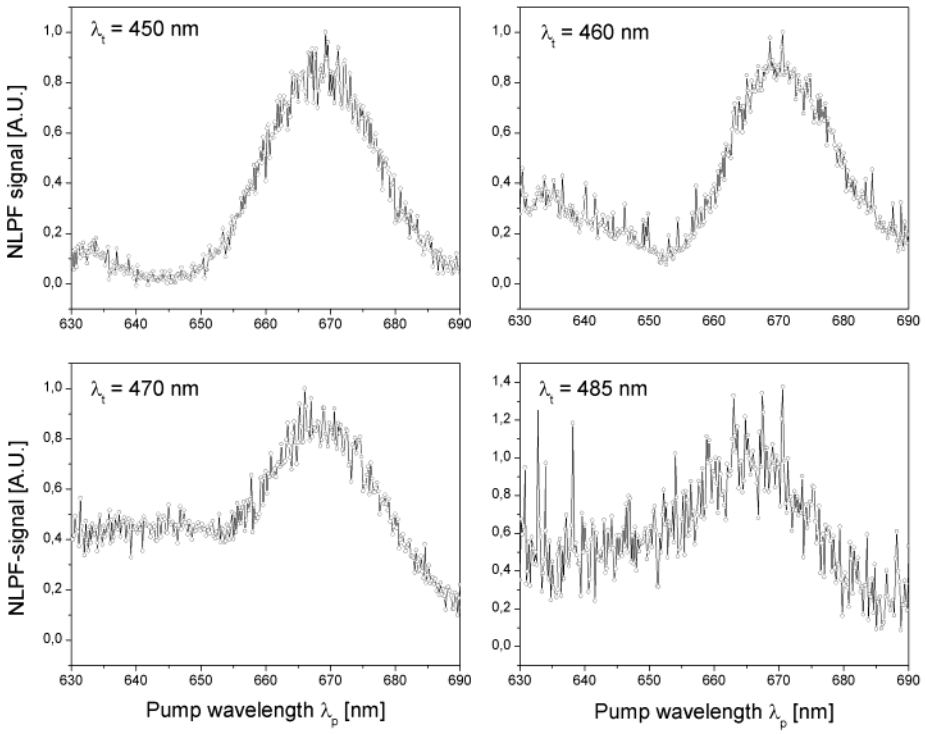

FIGURE 6: NLPF spectra of CP29 obtained at different probe wavelengths (λ_t) in the Soret region. All spectra were obtained at the same pump intensity.

bands, NLPF spectra pumped and probed in absorption bands with no spectral overlap were measured. Thus, λ_t was placed in the Chl Soret (and xanthophyll) absorption regions while pumping in the Q_y band.

NLPF spectra pumped in the Q_y region (640−700 nm) and probed at $\lambda_t = 450$ and 460 nm (essentially Chl *a* Soret region) as well as 470 and 485 nm (Chl *b* Soret and xanthophyll region) are displayed in Figure 6. Those contributions to the NLPF spectra, which originate from the Chl *b* partition of the Q_y band ($\lambda_p = 635-660$ nm) depend strongly on the position of λ_t and expectedly increase with shifting λ_t from the Chl *a* to the Chl *b* Soret region. On the other hand, all NLPF spectra exhibit, independent of the position of λ_t, a pronounced subband with a maximum around 670 nm. Noteworthy, the latter feature is observed even when λ_t is *beyond* the Chl *a* Soret absorption (above 460 nm). In other words, exciting Chl *a* low-energy Q_y states (between 670 and 690 nm) elicits a NLPF response in the (higher energy) Chl *b* Soret region. This observation can be hardly explained assuming noninteracting pigments but indicates *strong excitonic coupling* between certain Chls *a* and *b*. The observation that the center wavelength and line shape of this subband (located at around 670 nm) are almost unchanged upon variation of λ_t indicates that the respective coupled Chl *a* can be assigned to a subband peaking at 670 nm. Moreover, since there is no significant contribution of longer wavelength bands to the NLPF signal probed in the Chl *b* Soret region, the initial assumption of a subband (peaking at 681 nm) not being excitonically coupled to Chl *b* is confirmed.

At this point a possible contribution of theoretically predicted low dipole strength Chl *a* transitions between the Q_x and B_x regions (*20*, *21*) to the NLPF signal has to be discussed. Indeed, Chl *a* absorption is not zero in this region. However, although NLPF is a very sensitive technique, contributions from these states to the NLPF signal will be hardly detectable (since they are 2 orders of magnitude less intense absorbing than Chl *b* B_x). Moreover, whereas Chl *a* absorption slightly increases toward 500 nm, Chl *b* B_x absorption strongly decreases concomitantly with the decrease of the 670 nm NLPF subband intensity (not shown). Another issue that might complicate the interpretation of the NLPF spectra concerns possible contributions due to depletion of the ground state of xanthophyll molecules. However, previous studies with the related complex LHC II (*29*) indicate that population of xanthophyll excited states (via ^{3}Chl* → ^{3}xanthophyll* EET) in relation to the relevant Chl *a* ground state depletion is negligible under the described excitation conditions.

Additionally, by tuning the probe wavelength from 460 to 490 nm (and, hence, decreasing the ratio of Chl *b* to xanthophyll excitation), we observed a decline of the 670 nm NLPF signal, rendering a contribution due to interactions of Chl *a* and xanthophyll(s) unlikely.

Resolution of Spectral Substructure by Global Line-Shape Analysis. In the following section, a further analysis of spectral substructure in the Q_y region of CP29 is outlined. A global analysis of the total set of NLPF spectra obtained with λ_t in the Q_y region was performed. On the basis of the hints obtained so far, the following assumptions were taken into account: (i) The Q_y band of CP29 is heterogeneous (consists of yet unresolved subbands). (ii) At least two spectral subsystems have to be assumed. (iii) The red-most feature (peaking at about 681 nm) of the NLPF spectra can be assigned to one subband that is not excitonically coupled to any other subband. This is immediately obvious from a comparison of the line shape of the measured NLPF spectra with the theoretically predicted shape of a heterogeneous model system (compare Figure 3). (iv) To describe the Q_y region in the range below 680 nm, subband positions from the literature (*18*, *23*) were taken as starting parameters. (v)

Excitonic coupling between at least one Chl *a* and one Chl *b* subband was explicitly included in the models as suggested by the above considerations (compare NLPF spectra probed in the Soret region and pumped in the Q_y band). (vi) The subband of the excitonically coupled Chl *a* was assumed to be located at about 670 nm.

Out of the tested manifold of models constructed on the basis of the above assumptions, one fitted the available experimental data most consistently. The results can be summarized as follows: (i) The existence of the proposed band at the red-most edge of the Q_y band (at about 681 nm) is confirmed, being also in accordance to a previous mutational analysis (*30*). Remarkably, this band is found not to be coupled excitonically at room temperature as well as at 4 K as revealed by nonphotochemical hole-burning data (*22*) where the maximum of this band is located at 678 nm due to a cooling induced shift. However, a direct comparison of data as obtained at cryogenic temperatures and at (physiologically relevant) room temperature may not be warranted for several reasons. First of all, immersion of pigment−protein complexes in approximately 70% glycerol to facilitate freezing (usually at elevated concentrations of detergents to prevent glycerol-induced aggregation) may well bring about structural and spectral alterations of the samples, as well as the freezing process in itself (*17*). Moreover, low temperature can induce spectroscopic effects that may confound investigation of excitonic interactions. Spectral line narrowing at low temperature can decrease spectral overlap between neighboring chromophores and, hence, lessen excitonic interactions. Decreased optical dephasing (loss of excitonic coherence) at low temperature may, in contrast, enhance excitonic interactions (that may vanish at higher temperatures; see ref *31*). Further support for the existence of a nonexcitonically coupled band at the end of the EET chain in CP29 comes from comparison of stepwise two-photon-excited "blue" fluorescence spectra between CP29 and LHC II (*32*). Whereas two-photon excitation with 100 fs pulses in the Chl *a* Q_y region at 680 nm elicits fluorescence from the Chl *b* B_x state in LHC II, under the same excitation conditions only Chl *a* B_x fluorescence is observed in CP29 (*32*). (ii) Four further subbands (centered at 670, 660, 646, and 640 nm) are revealed. (iii) The bands at 670 (Chl *a*) and 640 nm (Chl *b*) are excitonically coupled.

An apparent discrepancy is observed as the result of fits assuming purely homogeneously broadened subbands, namely, only five subbands are resolved but eight Chls are bound to CP29. Taking additionally inhomogeneous broadening into account does not result in substantially altered subband characteristics, except for the 670 nm peaking species, indicating that the band consists of more than one (unresolved) Chl *a* species located at different binding sites.

Generally, models not taking strong excitonic coupling between at least two pigments into account totally failed.

Indications for excitonic coupling between Chls *a* and *b* in CP29 can be found in the literature. First, strong coupling of certain chromophores in CP29 is suggested by model calculations as presented in ref *12*. Second, ultrafast transient absorption experiments reveal instantaneous bleaching (within the limits of temporal resolution of the respective experiment) not only in the spectral region of the pump pulse (around 640 nm, Chl *b*) but also in the Chl *a* Q_y range (*11*, *12*). However, neither of these studies considered excitonic coupling between Chls *a* and *b* to explain the observed instantaneous Chls *a* bleaching. Rather, an attempt to simulate such ultrafast transient absorption data for excitation at 640 nm was made in the framework of incoherent Förster-type EET, which apparently failed (see ref *12*, Figure 5A,B, in remarkable contrast to 653 nm excitation). Excitation of higher vibronic levels of Chl *a* was invoked to explain concomitant bleaching in the Chl *a* region upon 640 nm pumping by these authors (*11*, *12*). However, the latter is not an issue in the described NLPF experiment and is easily circumvented with selective excitation (pumping) of the Chl *a* Q_y (0,0) transition and probing in the Chl *b* Soret band.

Summarizing the results and the above considerations on spectroscopy at cryogenic and ambient temperature, one can state that NLPF is a suitable technique to reveal excitonic interactions in pigment−protein complexes at physiological relevant temperatures.

CONCLUSIONS

The Chl *a*, Chl *b* Q_y absorption band substructure of the monomeric minor photosystem II antenna complex CP29 was investigated at room temperature by NLPF. The dominant Chl *a* absorption (with a maximum at 674 nm) splits into (at least) three subbands (centered at 660, 670, and 681.5 nm). In the Chl *b* spectral region two subbands with maxima at 640 and 646 nm can be identified. The lowest energy Chl *a* state (at 681.5 nm) is connected to other pigments only by Förster-type EET. Pronounced excitonic interactions exist between certain Chl *a* and Chl *b* molecules: the subbands at 640 and 670 nm (Chl *a/b*) constitute a strongly coupled pair. The above findings challenge the current view that essentially pigment−protein interactions are responsible for spectral heterogeneity in CP29.

REFERENCES

1. Jansson, S. (1994) *Biochim. Biophys. Acta 1184*, 1−19.
2. Paulsen, H. (1995) *Photochem. Photobiol. 62*, 367−382.
3. Horton, P., and Ruban, A. V. (1992) *Photosynth. Res. 34*, 375−385.
4. Härtel, H., and Lokstein, H. (1995) *Biochim. Biophys. Acta 1228*, 91−94.
5. Renger, G. (1992) in *The Photosystems: Structure, Function and Molecular Biology* (Barber, J., Ed.) pp 45−99, Elsevier Science Publishers, Amsterdam.
6. Van Grondelle, R., Dekker, J. P., Gillbro, T., and Sundström, V. (1994) *Biochim. Biophys. Acta 1187*, 1−65.
7. Mullineaux, C. W., Pascal, A. A., Horton, P., and Holzwarth, A. R. (1993) *Biochim. Biophys. Acta 1141*, 23−28.
8. Connelly, J. P., Müller, M. G., Hucke, M., Gatzen, G., Mullineaux, C. W., Ruban, A. V., Horton, P., and Holzwarth, A. R. (1997) *J. Phys. Chem. B 101*, 1902−1909.
9. Gradinaru, C. C., Özdemir, S., Gülen, D., van Stokkum, I. H. M., van Grondelle, R., and van Amerongen, H. (1998) *Biophys. J. 75*, 3064−3077.
10. Gradinaru, C. C., van Stokkum, I. H. M., Pascal, A. A., van Grondelle, R., and van Amerongen, H. (2000) *J. Phys. Chem. B 104*, 9330−9342.
11. Gradinaru, C. C., Pascal, A. A., Van Mourik, F., Robert, B., Horton, P., van Grondelle, R., and van Amerongen, H. (1998) *Biochemistry 37*, 9330−9342.
12. Cinque, G., Croce, R., Holzwarth, A., and Bassi, R. (2000) *Biophys. J. 79*, 1706−1717.
13. Kühlbrandt, W., Wang, D. N., and Fujiyoshi, Y. (1994) *Nature 367*, 614−621.
14. Renger, T., and May, V. (1997) *J. Phys. Chem. B 101*, 7232−7240.

15. Lokstein, H., Leupold, D., Voigt, B., Nowak, F., Ehlert, J., Hoffmann, P., and Garab, G. (1995) *Biophys. J. 69*, 1536−1543.
16. Beenken, W., and Ehlert, J. (1998) *J. Chem. Phys*. *109*, 10126−10137.
17. Leupold, D., Voigt, B., Beenken, W., and Stiel, H. (2000) *FEBS Lett. 480*, 73−78.
18. Giuffra, E., Zucchelli, G., Sandona, D., Croce, R., Cugini, D., Garlaschi, F. M., Bassi, R., and Jennings, R. C. (1997) *Biochemistry 36*, 12984−12993.
19. Pascal, A., Gradinaru, C., Wacker, U., Peterman, E., Calkoen, F., Irrgang, K.-D., Horton, P., Renger, G., van Grondelle, R., Robert, B., and van Amerongen, H. (1999) *Eur. J. Biochem. 262*, 817−823.
20. Parusel, A. B. J., and Grimme, S. (2000) *J. Phys. Chem. B 104*, 5395−5398.
21. Sundholm, D. (2000) *Chem. Phys. Lett. 317*, 545−552.
22. Pieper, J., Irrgang, K.-D., Rätsep, M., Voigt, J., Renger, G., and Small, G. J. (2000) *Photochem. Photobiol. 71*, 574−581.
23. Zucchelli, G., Dainese, P., Jennings, R. C., Breton, J., Garlaschi, F. M., and Bassi, R. (1994) *Biochemistry 33*, 8982−8990.
24. Scherz, A., and Parson, W. W. (1984) *Biochim. Biophys. Acta 766*, 666−678.
25. Berthold, D. A., Babcock, G. T., and Yocum, C. F. (1981) *FEBS Lett. 134*, 231−234.
26. Völker, M., Ono, T., Inoue, Y., and Renger, G. (1985) *Biochim. Biophys. Acta 806*, 25−34.
27. Henrysson, T., Schröder, W. P., Spangfort, M., and Akerlund, H.-E. (1989) *Biochim. Biophys. Acta 977*, 301−308.
28. Voigt, B., Nowak, F. R., and Beenken, W. (1999) *Meas. Sci. Technol. 10*, N7−N11.
29. Schödel, R., Irrgang, K.-D., Voigt, J., and Renger, G. (1999) *Biophys. J. 76*, 2238−2248.
30. Bassi, R., Croce, R., Cugini, D., and Sandona, D. (1999) *Proc. Natl. Acad. Sci. U.S.A. 96*, 10056−10061.
31. Schubert, A., Voigt, B., Leupold, D., Beenken, W., Ehlert, J., Hoffmann, P., and Lokstein, H. (1997) *Biochim. Biophys. Acta 1321*, 195−199.
32. Leupold, D., Teuchner, K., Ehlert, J., Irrgang, K.-D., Renger, G., and Lokstein, H. (2002) *Biophys. J.* (in press).

BI0155854